



HHS Public Access

Author manuscript

ACS Chem Biol. Author manuscript; available in PMC 2018 August 18.

Published in final edited form as:

ACS Chem Biol. 2018 August 17; 13(8): 2161–2169. doi:10.1021/acscchembio.8b00336.

Halo Tag Assay Suggests Common Mechanism of *E. coli* Membrane Permeabilization Induced by Cationic Peptides

Zhilin Yang and James C. Weisshaar*

Department of Chemistry and Molecular Biophysics Program University of Wisconsin-Madison

Abstract

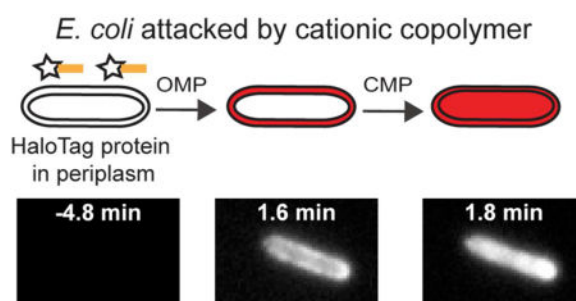
Permeabilization of the Gram negative bacterial outer membrane (OM) by antimicrobial peptides (AMPs) is the initial step enabling access of the AMP to the cytoplasmic membrane. We present a new single-cell, time-resolved fluorescence microscopy assay that reports on the permeabilization of the *E. coli* OM to small molecules, with time resolution of 3 sec or better. When the profluorophore JF₆₄₆ (702 Da) crosses the outer membrane (OM) and gains access to the periplasm, it binds to localized HaloTag protein (34 kDa) and fluoresces in a characteristic hollow spatial pattern. Previous work used the much larger periplasmic GFP (27 kDa) probe, which reports on OM permeabilization to globular proteins. We test the assay on three cationic agents: the Gellman random β -peptide copolymer MM₆₃:CH_{x37}, the human AMP LL-37, and the synthetic hybrid AMP CM15. These results combined with previous work suggest a unifying sequence of OM and cytoplasmic membrane (CM) events that may prove commonplace in the attack of cationic peptides on Gram negative bacteria. The peptide initially induces gradual OM permeabilization to small molecules, likely including the peptide itself. After a lag time, abrupt permeabilization of the OM, abrupt re-sealing of the OM, and abrupt permeabilization of the CM (all to globular proteins) occur in rapid sequence. We propose a mechanism based on membrane curvature stress induced by time-dependent differential binding of peptide to the outer leaflet of the OM and CM. The results provide fresh insight into the critical OM permeabilization step leading to a variety of damaging downstream events.

TOC image

*Corresponding author: weisshaar@chem.wisc.edu.

SUPPORTING INFORMATION

Supporting Information *Available*: This material is available free of charge *via* the Internet. Details on methods, strains and plasmids used in this work (Table S1). Control experiments for the HaloTag-based membrane permeabilization assay (Figure S1). Histograms of lag times for one-color experiment after MM₆₃:CH_{x37} addition (Figure S2). An example of two-color experiment after LL-37 addition (Figure S3). Five movies under various conditions.



Antimicrobial peptides (AMPs), also called host-defense peptides, play a dual role in the innate immune system of many species, including humans, acting as both antimicrobial agents and signaling molecules.^{1,2} In this era of multi-drug resistant bacteria, AMPs may serve as useful lead compounds in the search for novel antibacterial agents. One widespread mechanism of action of natural AMPs is the permeabilization of bacterial membranes of both Gram positive and Gram negative species. Perhaps as a result, bacterial resistance to AMPs develops only slowly.

By now it is clear that the damage mechanisms induced by AMPs go well beyond membrane permeabilization and destruction of the trans-membrane potential that drives ATP production.^{3,4} A wide variety of bulk culture and single-cell diagnostic assays have revealed numerous physical and biochemical effects of AMPs on cultured bacteria.^{5,6} Our lab has been developing single-cell, time resolved, fluorescence-based assays that monitor a variety of AMP-induced “symptoms”.⁷⁻¹⁵ We have focused primarily on the Gram negative species *E. coli* under attack by the polycationic AMPs LL-37,^{7,14} Cecropin A,⁸ CM15,¹¹ and Melittin,¹⁵ as well as by the synthetic cationic random β -peptide copolymer MM₆₃:CHx₃₇ (Table 1).¹³ Thus far the methods enable direct determination of the timing of events such as outer membrane permeabilization (OMP) to GFP, cytoplasmic membrane permeabilization (CMP) to GFP and a Sytox dye, cell shrinkage, the halting of growth, and the onset of oxidative stress. Each antimicrobial agent exhibits a unique set of events.

Our simplest assay uses a strain of *E. coli* MG1655 that expresses GFP bound to a TorA signal sequence, causing export of GFP from the cytoplasm to the periplasm via the Tat system.¹⁶ Periplasmic GFP creates a hollow, shell-like image in the 2D fluorescence microscope. This assay alone yields a surprising variety of behaviors for different cationic peptides. After initiation of the flow of LL-37,¹⁴ or Cecropin A⁸ across plated cells at $t = 0$, we observe a time lag followed by loss of the periplasmic GFP signal to the cell surround. The behavior is illustrated for a representative septating cell during attack by Cecropin A in Figure 1A. Evidently the AMP has induced OM permeabilization to small, globular proteins in localized fashion at the septal region. In sharp contrast, for the short, synthetic AMP CM15 and for the longer synthetic copolymer MM₆₃:CHx₃₇, the initial periplasmic GFP image abruptly evolves to a filled, cytoplasmic image. This alternative behavior is illustrated for a non-septating cell attacked by the copolymer in Figure 1B. Evidently the copolymer has first induced CM permeabilization to periplasmic GFP, which moves inward to fill the much larger cytoplasmic volume. Meanwhile, the total GFP fluorescence intensity remains essentially constant. GFP is lost to the surround only much later. Most recently, we found

that Melittin induces behavior intermediate between that of Figure 1A and 1B.¹⁵ After a time lag, roughly half of the periplasmic GFP intensity is lost to the surround, and the remainder of the intensity soon exhibits a cytoplasmic spatial distribution. Complete loss of GFP occurs only much later. Evidently the OM has become transiently permeable to GFP and then re-sealed. Meanwhile the CM has become permeable to GFP. Such re-sealing behavior is reminiscent of the effects of AMPs on purified lipid vesicles and GUVs.¹⁷⁻²⁴

GFP is a small, globular protein of mass 27 kDa, much larger than the typical antimicrobial agent of mass ~1-5 kDa. Before periplasmic GFP has moved inward to fill the cytoplasm, the antimicrobial agent must surely have translocated across the OM to gain access to the periplasmic space and to the CM itself. This passage is the key initial step in AMP activity against Gram negative bacteria. An important mechanistic question is: how does the cationic agent cross the OM? It is possible that linear cationic peptides might thread their way through open porin channels in the OM, as seemingly occurs for colicin.²⁵ The peptide might also transiently insert in the OM bilayer and subsequently de-insert into the periplasmic space, without having permeabilized the OM to other small molecules, much less to GFP. Finally, the peptide might first induce OM permeabilization to smaller species, including itself; these permeabilization sites may subsequently evolve to enable passage of small globular proteins such as GFP.

In order to dissect these possibilities, it is highly desirable to develop a single-cell assay that detects the onset of OM permeabilization to small molecules with good time resolution. Previously developed bulk assays used small profluorophores to detect permeabilization of the OM, but without spatiotemporal resolution.²⁶⁻²⁸ Here we describe a single-cell, time-resolved, fluorescence microscopy assay based on binding of a red-emitting profluorophore called JF₆₄₆ ligand²⁹ (mass 702 Da, Figure 2B) to HaloTag protein³⁰ (34 kDa) that has been exported to the periplasm. When an antimicrobial agent induces OM permeabilization to the JF₆₄₆ ligand, the ligand gains access to the periplasm, binds covalently to HaloTag protein, and fluoresces red with a periplasmic spatial distribution. The assay is sensitive enough to detect the onset of OM permeabilization to JF₆₄₆ ligand with time resolution of 3 sec or better. The new results for copolymer MM₆₃:CHx₃₇ and for LL-37 strongly suggest that a common mechanism may apply to all five peptides in Table 1. Initial, gradual OM permeabilization to small species is followed by a time lag before abrupt OM permeabilization to globular proteins. Abrupt re-sealing of the OM and permeabilization of the CM to globular proteins follow shortly afterward. This may prove to be a fairly general sequence of events across a variety of cationic peptides, with timing details dependent on the specific peptide and its concentration. We present a mechanistic picture of membrane permeabilization and re-sealing in terms of time-dependent curvature stress caused by asymmetric binding of the peptide to the two leaflets of the membrane. This mechanism is borrowed from a large body of work on vesicles composed of pure lipids.¹⁷⁻²²

Future extensions might combine the new HaloTag-based assay with addition of external Sytox Green or Sytox Orange, which bind to chromosomal DNA to signal CM permeabilization to small molecules. Such a combined single-cell assay could reveal the timing of OM and CM permeabilization events to both small species and globular proteins,

all in one experiment. These methods may also find application in mechanistic studies of the effects of small-molecule antibiotics.

RESULTS AND DISCUSSION

The new assay detects the onset of OM permeabilization to small molecules using the HaloTag concept (Figure 2).³⁰ This requires two components, an *E. coli* strain that exports the HaloTag protein to the periplasmic space and an impermeant profluorophore called JF₆₄₆ ligand.²⁹ The strains used in this work are listed in Table S1. Strain zy3720 carries a plasmid pMB2 that expresses HaloTag protein with the DsbA signal peptide appended to the N-terminus (ssDsbA-HaloTag). As a result, HaloTag protein is co-translationally exported to the periplasm, as previously shown.³¹ In aqueous solution, the JF₆₄₆ ligand preferentially adopts the closed lactone form, which fluoresces only weakly (Figure 2B). When JF₆₄₆ ligand binds covalently to the HaloTag protein to form the HaloTag-JF₆₄₆ conjugate, the local environment around JF₆₄₆ changes. The result is a large increase in red JF₆₄₆ fluorescence.^{29,32} A hollow, shell-like spatial distribution signals the passage of JF₆₄₆ ligand across the OM into the periplasm. At the same time, the OM presumably becomes permeable to other small molecules, likely including the antimicrobial agent itself. If the next step is CM permeabilization to globular proteins, the HaloTag-JF₆₄₆ conjugate gains access to the cytoplasm, and the hollow spatial distribution fills in. If the next step is OM permeabilization to globular proteins, the conjugate leaves the cell envelope and the red fluorescence disappears. By measuring fluorescence intensity across the short axis of the cell, we can determine for each camera frame whether a fluorophore distributes predominantly in the periplasm or throughout the entire cell.

Minimum inhibitory concentration (MIC) results for the antimicrobial agents are shown in Table 1. Details of the microscopy experiments are described in SI. Briefly, exponentially growing cells are plated in a microfluidics chamber. At $t = 0$, the flow of aerated medium is switched to aerated medium plus a fixed concentration of antimicrobial agent and 100 nM JF₆₄₆ ligand. For one-color imaging experiments using strain zy3720, we alternate fluorescence and phase contrast images, usually at 6 sec intervals (12 sec/cycle). The fluorescence image monitors the JF₆₄₆ ligand binding to HaloTag protein and the phase contrast image monitors cell length. Two-color imaging experiments use strain zy3722 that contains a plasmid expressing both ssDsbA-HaloTag and ssTorA-GFP. Both HaloTag protein and GFP are exported to the periplasm. We sequentially acquire two fluorescence channels and the phase contrast channel, again at 12 sec/cycle. The green channel monitors GFP, the red channel monitors JF₆₄₆ fluorescence, and the phase contrast channel monitors cell length. For each case, typically at least 60 cells in total were analyzed from three repeat experiments.

Preliminary tests

First we tested two strains for their ability to export HaloTag protein to the periplasm, zy3719 and zy3720 (Table S1). Strain zy3719 carries plasmid pMB1, expressing the HaloTag domain fused to the signal sequence of maltose-binding periplasmic protein (ssMalE-HaloTag). Strain zy3720 carries plasmid pMB2, expressing the HaloTag domain

fused to the signal sequence of the periplasmic protein DsbA (ssDsbA-HaloTag). To determine where the HaloTag protein localizes inside *E. coli* cells, we added the permeable, red fluorescent tetramethylrhodamine ligand (TMR ligand).³⁰ On excitation at 561 nm, TMR ligand emits at 580 nm. When supplied exogenously, TMR ligand permeates both membranes of living *E. coli* cells and covalently binds to HaloTag protein specifically. After rinsing with fresh medium, unbound TMR ligands are removed from the cells. The pattern of the residual fluorescence reports on the spatial distribution of the HaloTag protein.

Wild-type (WT) MG1655 cells do not express HaloTag protein and exhibited no significant TMR fluorescence after TMR ligand incubation and rinsing (Figure S1A). There is little or no permanent binding of TMR ligand to the cell envelope or to periplasmic or cytoplasmic components. Attempts at exporting HaloTag protein to the periplasm using ssMalE (strain zy3719) failed (Figure S1A). TMR fluorescence fills the entire cell, indicating that functional HaloTag protein remains primarily in the cytoplasm. In contrast, for strain zy3720 using the ssDsbA signal, TMR fluorescence exists predominately in the periplasm, indicating that HaloTag protein is exported efficiently to the periplasm (Figure S1A). Similarly, two-color imaging demonstrated that strain zy3722 efficiently exports both HaloTag protein and GFP to the periplasm (Figure S1A).

Next we tested the membrane permeability and toxicity of JF₆₄₆ ligand towards *E. coli*. At $t = 0$, we flowed 100 nM JF₆₄₆ ligand alone across *E. coli* zy3720 cells expressing periplasmic HaloTag protein. Fluorescence images and phase contrast images were interleaved, to monitor JF₆₄₆ fluorescence and bacterial growth. During 1 hr of continuous flow, no obvious fluorescence was observed inside the cells (Figure S1B, Movie S1). Although some background fluorescence outside the cells appeared in the first few minutes, JF₆₄₆ ligand at 100 nM does not permeate the OM of *E. coli*. A detailed description is included in SI. Meanwhile, JF₆₄₆ ligand does not harm the growth of *E. coli*, as cells continue to grow and divide. The doubling time for *E. coli* zy3720 cells in the presence of 100 nM JF₆₄₆ ligand is 52 ± 3 min, determined from cell length vs time. This is comparable to the 50 ± 3 min doubling time of WT *E. coli* cells plated in the microfluidic chamber when only EZ rich defined medium (EZRD) is supplied.

Finally, we tested for JF₆₄₆ fluorescence in WT cells (lacking HaloTag protein) after permeabilization by copolymer MM₆₃:CHx₃₇ at 1.2X MIC (Figure S1C). We observe only a weak burst of red intracellular fluorescence that begins after OM permeabilization (see below) and quickly dies away. This burst is at least 30-fold weaker than the JF₆₄₆ fluorescence induced in zy3720 cells by the copolymer, as shown below.

Membrane permeabilization and re-sealing induced by copolymer MM₆₃:CHx₃₇

First we used the one-color assay to observe membrane permeabilization events induced by the copolymer MM₆₃:CHx₃₇ in *E. coli* cells. At $t = 0$, we flowed 30 μ g/mL of MM₆₃:CHx₃₇ (1.2X MIC) plus 100 nM JF₆₄₆ ligand across plated *E. coli* zy3720 cells that export HaloTag protein to the periplasm. In these one-color experiments, we monitored JF₆₄₆ fluorescence and phase contrast every 12 s. Consistent with our previous study,¹³ nearly all cells began to shrink in length beginning within 24 sec of MM₆₃:CHx₃₇ addition. Later some cells partially recovered cell length, as before. For the representative cell in Figure 3A and Movie S2, the

cell length decrease started at $t_1 = 0.2$ min and continued until 1.4 min, when partial reversal occurred. Beginning at $t_2 = 0.4$ min, red JF₆₄₆ fluorescence increased abruptly and continued to rise until $t = 1.8$ min, when it reached a plateau (Figure 3C). The plateau may indicate that all the HaloTag protein has become bound by JF₆₄₆ ligands. As shown from transverse intensity profiles (Figure 3B), the JF₆₄₆ fluorescence at first accumulated in the periplasm, but began to fill the cytoplasm at $t_3 = 1.6$ –1.8 min.

Copolymer MM₆₃:CHx₃₇ caused OM permeabilization to JF₆₄₆ ligand, allowing it to enter the periplasm and bind to the HaloTag protein. Initially much or all of the HaloTag-JF₆₄₆ conjugate remained in the periplasm. Later the CM was permeabilized to the HaloTag-JF₆₄₆ conjugate, which began to fill the cytoplasm. Meanwhile, the OM remained essentially impermeable to the conjugate. We previously interpreted the shrinkage event as primarily an osmotic effect caused by entry of the highly cationic copolymer and its many counterions into the periplasm.¹³ The partial recovery of length may be due to import of K⁺ ions into the cytoplasm. Under the assumption that the OM was permeabilized to the copolymer (mean molar mass ~7 kDa) at the same time as the JF₆₄₆ ligand (702 Da), the earlier explanation is corroborated. Notice that the onset of shrinkage matches the onset of HaloTag-JF₆₄₆ conjugate fluorescence within 1 camera cycle = 0.2 min = 12 sec. The duration of the shrinkage event and the risetime of the fluorescence seem to match as well.

It is important to exclude the possibility that the JF₆₄₆ fluorescence increase is produced by interaction of JF₆₄₆ ligand with some intracellular species other than HaloTag protein. In Figure S1C (and Movie S3), we show a control experiment flowing 30 μ g/mL MM₆₃:CHx₃₇ plus 100 nM JF₆₄₆ ligand across wild type *E. coli* cells containing no HaloTag protein. A weak, transient, intracellular, cytoplasmic signal appears only after the shrinkage event. The peak fluorescence intensity in the control experiments (Figure S1C) is at least 30-fold smaller than the plateau value attained when HaloTag protein is present (Figure 3C). Evidently the bright periplasmic fluorescence observed in zy3720 cells is almost entirely due to the binding of JF₆₄₆ ligand to the HaloTag protein following OM permeabilization.

We measure the mean values across cells of the timing events t_1 (onset of cell shrinkage), ($t_2 - t_1$) (the additional lag time to the onset of HaloTag-JF₆₄₆ conjugate fluorescence in the periplasm), and ($t_3 - t_2$) (the lag time between the onset of periplasmic fluorescence and entry of the conjugate into the cytoplasm). The corresponding detailed distributions are shown in Figure S2. Across 70 cells, $\langle (t_2 - t_1) \rangle = 0.2 \pm 0.0$ min and $\langle (t_3 - t_2) \rangle = 1.0 \pm 0.7$ min ($\pm 1SD$). Even at 1.2X MIC, the Gellman copolymer MM₆₃:CHx₃₇ permeabilizes the OM and CM in rapid succession. The new assay readily discerns both the onset of OM permeabilization to small molecules and the onset of CM permeabilization to globular proteins using a single fluorophore.

To gain additional information, we also applied the two-color assay to the attack of copolymer MM₆₃:CHx₃₇ on *E. coli* cells. At $t = 0$, we flowed 30 μ g/mL MM₆₃:CHx₃₇ (1.2X MIC) plus 100 nM JF₆₄₆ ligand across *E. coli* zy3722 cells that export both HaloTag protein and GFP to the periplasm. In these experiments, we monitored green GFP fluorescence, red JF₆₄₆ fluorescence, and phase contrast with a cycle time of 12 s. As in the one-color experiment, the JF₆₄₆ signal begins to rise shortly after the onset of cell shrinkage,

initially forming a periplasmic image. For the particular cell in Figure 4A and Movie S4, this occurs at $t_2 = 0.6$ min, and the signal continues to rise gradually up until $t_3 = 5.2$ min. The JF₆₄₆ image remains periplasmic during this interval. Meanwhile, the periplasmic GFP image maintains its intensity (except for minor photobleaching) over the same period. This demonstrates clearly that the OM has initially become permeabilized to small molecules such as JF₆₄₆ ligand, but not to small globular proteins such as periplasmic GFP.

At $t_3 = 5.2$ min, both GFP and JF₆₄₆ images abruptly change from periplasmic to cytoplasmic. Interestingly, at the same moment the GFP intensity decreases by about 10% while the HaloTag-JF₆₄₆ conjugate intensity increases by about 20%. Our interpretation is that the copolymer is inducing transient permeabilization of the OM to GFP, after which the OM re-seals to globular proteins of GFP size or larger. The transient opening lasts only about 3 frames = 36 sec. The same transient OM permeabilization event presumably also releases some of the (slightly larger) periplasmic HaloTag protein. However, during the transient event, the JF₆₄₆ ligand can cross the OM more rapidly than before, resulting in a net abrupt increase in fluorescence from the HaloTag-JF₆₄₆ conjugate. Essentially simultaneously with the OM re-sealing event, the CM becomes permeable to both GFP and HaloTag-JF₆₄₆ conjugate and both images fill in. Meanwhile, the OM remains permeable to JF₆₄₆ ligand, as evidenced by the slow continuing rise of conjugate fluorescence at $t > 5.2$ min.

Membrane permeabilization and re-sealing induced by LL-37

We also applied the one-color assay to the human AMP LL-37. In previous work imaging periplasmic GFP and Sytox Green in the same fluorescence channel, we had observed loss of roughly 90% of periplasmic GFP to the surround (signaling OM permeabilization to GFP) and the subsequent rise in Sytox Green fluorescence (CM permeabilization to Sytox Green).^{7,14} The very strong Sytox Green signal would have obscured any residual GFP that was trapped inside the cell by a membrane re-sealing event.

The one-color HaloTag assay reveals that an OM re-sealing event in fact occurs during the attack of LL-37. At $t = 0$ we initiated flow of 4 μ M LL-37 (1X MIC) plus 100 nM JF₆₄₆ across plated zy3720 cells. The typical behavior is shown in Figure 5 and Movie S5. Within 2 min, an intracellular, periplasmic signal from HaloTag-JF₆₄₆ conjugate begins to rise gradually and cell growth begins to slow down. At $t = 14.5$ min, some 75% of the fluorescence is lost abruptly to the surround. The remaining 25% exhibits the cytoplasmic (filled cell) spatial pattern. Once again, our interpretation is that the OM is transiently permeabilized to the conjugate. At essentially the same time as the OM re-seals to globular proteins, the CM is permeabilized to the conjugate. A brief test of the two-color assay (green periplasmic GFP and red HaloTag-JF₆₄₆ conjugate) on LL-37 confirmed that periplasmic GFP and HaloTag-JF₆₄₆ conjugate move similarly in space and time (Figure S3). Most of the GFP and the conjugate intensity is lost at the same time, and both images change abruptly from the periplasmic to the cytoplasmic spatial distribution.

Rapid CM permeabilization induced by CM15

Finally, we applied the one-color assay to the short, synthetic antimicrobial peptide CM15, which was previously shown to induce very rapid migration of periplasmic GFP into the cytoplasm.¹¹ Flow of 10 μ M CM15 (2X MIC) plus 100 nM JF₆₄₆ ligand across zy3720 cells began at $t = 0$. In an attempt to estimate the kinetic response time of the new assay, the time resolution was increased to 3 sec/cycle. For the representative cell in Figure 6, shrinkage of cell length by some 20% began abruptly at $t_1 = 39$ sec and was essentially complete in only 4 frames = 12 sec. The onset of JF₆₄₆ fluorescence was essentially simultaneous with t_1 . We infer very rapid passage of CM15 across the OM and into the periplasm. Evidently the assay is sufficiently sensitive to detect the onset of OM permeabilization to small molecules to within 3 sec or better. The shift of JF₆₄₆ fluorescence from a periplasmic distribution to a cytoplasmic distribution occurs within one camera cycle, at $t_2 = 0.70$ - 0.75 min = 42-45 sec. This event is also detected with time resolution of 3 sec or better. The rising signal reached 2/3 of its plateau value in 10 frames = 30 sec. This is a convolution of the timescale of passage of JF₆₄₆ ligand into the periplasm and the timescale for the bimolecular reaction between JF₆₄₆ ligand and the periplasmic HaloTag protein. Thus we take 30 sec as an upper bound on the kinetic response time of the new assay under the conditions described. The comparable fluorescence risetime for the copolymer experiment in Figure 3C is much longer, ~60 sec. Accordingly, the cell shrinkage event is slower, itself requiring ~60 sec. We interpret this to mean that the copolymer and JF₆₄₆ ligand gain access to the periplasm less rapidly than do CM15 and JF₆₄₆ ligand.

General mechanistic insights

The new HaloTag-JF₆₄₆ assay reveals that after an initial time delay, both the copolymer MM₆₃:CHx₃₇ and the natural AMP LL-37 induce a brief period of OM permeability to globular proteins followed by re-sealing of the OM and abrupt permeabilization of the CM to globular proteins. A similar sequence of events was recently elucidated for the antimicrobial peptide Melittin using periplasmic GFP as the probe.¹⁵ For MM₆₃:CHx₃₇ and for LL-37, the new HaloTag assay also enables direct observation of permeabilization of the OM to the much smaller JF₆₄₆ ligand during the initial lag time leading up to OM permeabilization to globular proteins. It is highly likely that the OM has become permeable to the antimicrobial agent itself during the same initial period. We have not tested the timing of JF₆₄₆ permeability induced by Melittin.

Evidently all three of these cationic peptides attack the *E. coli* cell envelope in a similar sequence of mechanistic steps. During the initial period, the peptide binds to and penetrates the anionic lipopolysaccharide (LPS) layer, eventually permeabilizing the OM to small molecules such as JF₆₄₆ ligand, and presumably to the peptide itself. Our methods do not directly speak to the molecular-level details of the initial permeabilization mechanism, which could involve “detergent-like” disruption of OM structure^{33,34} or formation of small toroidal pores.^{35,36} It would be interesting to learn whether the initial permeabilization occurs locally or globally; such observations would require faster imaging than we have employed here. As more and more cationic peptide binds to the outer leaflet of the OM, this generates increasing curvature stress. The stress eventually causes abrupt OM permeabilization to globular proteins such as GFP, HaloTag protein, and the HaloTag-JF₆₄₆

conjugate, enabling partial loss to the cell surround. This larger-scale disruption of the OM begins and ends abruptly in comparison with the earlier, gradual, continual leakage of small molecules across the OM. Earlier work showed that the larger disruption is often localized at curved membrane surfaces; see the septating cell attacked by Cecropin A in Figure 1. These details suggest a slow nucleation event preceding the formation of pores sufficiently large to pass globular proteins. The larger-scale disruption event then enables much more rapid translocation of the peptide into the periplasm, where it binds to the inner leaflet of the OM. This relieves the curvature stress and enables effective re-sealing of the OM to globular proteins.

During the disruption of the OM to globular proteins, the peptide concentration can build rapidly in the periplasm. The same process of differential curvature stress repeats itself due to peptide binding to the outer leaflet of the CM, which then abruptly becomes permeable to globular proteins. The proteins that did not escape the periplasm during the transient OM permeabilization event thus gain entry to the cytoplasm. The rapid build-up of peptide concentration in the periplasm while the OM is open to passage of globular proteins explains why OM re-sealing and CM permeabilization to such proteins seem coupled in time. In the specific case of Melittin, detailed analysis showed that subsequently the CM also re-sealed to GFP, presumably by the same curvature relief mechanism. Seemingly analogous peptide-induced permeabilization and re-sealing events have been observed in studies of pure lipid vesicles and GUVs. Indeed, we have borrowed the curvature stress mechanism from that body of work¹⁷⁻²⁴

This detailed mechanistic picture of gradual permeabilization of the OM to small molecules followed by abrupt, transient permeabilization of the OM to globular proteins followed by permeabilization of the CM may prove to be fairly general in describing the attack of cationic peptides on *E. coli*, and perhaps on other Gram negative species as well. Similarly detailed studies of additional AMPs would test the generality of these events. Previous work shows that the timing of such events depends on the bulk peptide concentration.^{7,8} It is easy to imagine that different peptides will carry out these events at different rates. The HaloTag assay described here provides a new way to probe size- and time-dependent membrane permeabilization events in living cells in real time.

METHODS

The strains and plasmids used in this study are summarized in Table S1. Details of strain construction and induction conditions are provided in SI. Bulk cultures were grown in EZRDM³⁷ from glycerol frozen stock to stationary phase overnight at 30°C. Subcultures were grown to exponential phase (OD = 0.2-0.6 at 600 nm) before sampling for the microscopy experiments at 30°C. The antimicrobial agents are described in Table 1; additional details are found in SI. The aerobic MIC values for the various antimicrobial agents were determined using the broth microdilution method as previously described.⁷ Imaging of individual cells was carried out at 30°C in a simple microfluidics chamber as previously described.¹¹ Fresh, aerated medium flows over the cells continuously. The cells were imaged for ~5 min before switching to fresh medium containing the compounds under study (antimicrobial agent, JF₆₄₆ ligand). Details of the microscopy procedure and setup are

in SI. The concentration of each peptide was chosen to be sufficiently high to cause significant antimicrobial action on a 30-min timescale, but low enough to enable the methods to resolve sequential events in time.

Supplementary Material

Refer to Web version on PubMed Central for supplementary material.

Acknowledgments

We thank B. Mehmet (New England Biolabs) for providing the plasmids pMB1 and pMB2, L. Lavis (Janelia Research Campus) for providing JF₆₄₆ ligand, and H. Choi (Janelia Research Campus) for helpful discussion. The Gellman lab provided the MM₆₃:CH₃₇ copolymer sample.

FUNDING SOURCES

This research was supported by the National Institute of General Medical Sciences of the National Institutes of Health under awards R01GM094510 (to JCW as PI) and R01GM093265 (to JCW and Samuel Gellman as co-PIs). The content is solely the responsibility of the authors and does not necessarily represent the official views of the National Institutes of Health.

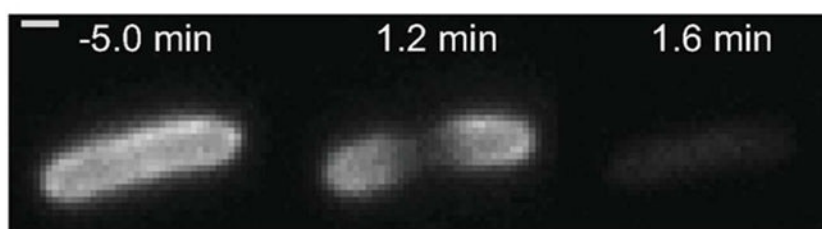
References

1. Zasloff M. Antimicrobial peptides of multicellular organisms. *Nature*. 2002; 415:389–395. [PubMed: 11807545]
2. Wimley WC, Hristova K. Antimicrobial peptides: successes, challenges and unanswered questions. *J Membr Biol*. 2011; 239:27–34. [PubMed: 21225255]
3. Brogden KA. Antimicrobial peptides: pore formers or metabolic inhibitors in bacteria? *Nat Rev Microbiol*. 2005; 3:238–250. [PubMed: 15703760]
4. Hancock RE, Sahl HG. New strategies and compounds for anti-infective treatment. *Current opinion in microbiology*. 2013; 16:519–521. [PubMed: 23998895]
5. Munoz A, Read ND. Live-cell imaging and analysis shed light on the complexity and dynamics of antimicrobial Peptide action. *Front Immunol*. 2012; 3:248. [PubMed: 22912634]
6. Choi H, Rangarajan N, Weisshaar JC. Lights, camera, action! Antimicrobial peptide mechanisms imaged in space and time. *Trends Microbiol*. 2016; 24:111–122. [PubMed: 26691950]
7. Sochacki KA, Barns KJ, Bucki R, Weisshaar JC. Real-time attack on single *Escherichia coli* cells by the human antimicrobial peptide LL-37. *Proc Natl Acad Sci US A*. 2011; 108:E77–81.
8. Rangarajan N, Bakshi S, Weisshaar JC. Localized permeabilization of *E. coli* membranes by the antimicrobial peptide Cecropin A. *Biochemistry*. 2013; 52:6584–6594. [PubMed: 23988088]
9. Barns KJ, Weisshaar JC. Real-time attack of LL-37 on single *Bacillus subtilis* cells. *Biochim Biophys Acta*. 2013; 1828:1511–1520. [PubMed: 23454084]
10. Bakshi S, Choi H, Rangarajan N, Barns KJ, Bratton BP, Weisshaar JC. Nonperturbative imaging of nucleoid morphology in live bacterial cells during an antimicrobial peptide attack. *Appl Environ Microbiol*. 2014; 80:4977–4986. [PubMed: 24907320]
11. Choi H, Yang Z, Weisshaar JC. Single-cell, real-time detection of oxidative stress induced in *Escherichia coli* by the antimicrobial peptide CM15. *Proc Natl Acad Sci USA*. 2015; 112:E303–310. [PubMed: 25561551]
12. Barns KJ, Weisshaar JC. Single-cell, time-resolved study of the effects of the antimicrobial peptide alamethicin on *Bacillus subtilis*. *Biochim Biophys Acta*. 2016; 1858:725–732. [PubMed: 26777771]
13. Choi H, Chakraborty S, Liu R, Gellman SH, Weisshaar JC. Single-cell, time-resolved antimicrobial effects of a highly cationic, random nylon-3 copolymer on live *Escherichia coli*. *ACS Chem Biol*. 2016; 11:113–120. [PubMed: 26493221]

14. Choi H, Yang Z, Weisshaar JC. Oxidative stress induced in *E. coli* by the human antimicrobial peptide LL-37. *PLoS Pathog.* 2017; 13:e1006481. [PubMed: 28665988]
15. Yang Z, Choi H, Weisshaar JC. Melittin-induced permeabilization, re-sealing, and re-permeabilization of *E. coli* Membranes. *Biophys J.* 2018; 114:368–379. [PubMed: 29401434]
16. Sochacki KA, Shkel IA, Record MT, Weisshaar JC. Protein diffusion in the periplasm of *E. coli* under osmotic stress. *Biophys J.* 2011; 100:22–31. [PubMed: 21190653]
17. Rex S, Schwarz G. Quantitative studies on the Melittin-induced leakage mechanism of lipid vesicles. *Biochemistry.* 1998; 37:2336–2345. [PubMed: 9485380]
18. Gregory SM, Pokorny A, Almeida PF. Magainin 2 revisited: a test of the quantitative model for the all-or-none permeabilization of phospholipid vesicles. *Biophys J.* 2009; 96:116–131. [PubMed: 19134472]
19. Krauson AJ, He J, Wimley WC. Determining the mechanism of membrane permeabilizing peptides: identification of potent, equilibrium pore-formers. *Biochim Biophys Acta.* 2012; 1818:1625–1632. [PubMed: 22365969]
20. Wiedman G, Herman K, Searson P, Wimley WC, Hristova K. The electrical response of bilayers to the bee venom toxin melittin: evidence for transient bilayer permeabilization. *Biochim Biophys Acta.* 2013; 1828:1357–1364. [PubMed: 23384418]
21. Cruz J, Mihailescu M, Wiedman G, Herman K, Searson PC, Wimley WC, Hristova K. A membrane-translocating peptide penetrates into bilayers without significant bilayer perturbations. *Biophys J.* 2013; 104:2419–2428. [PubMed: 23746514]
22. Savini F, Bobone S, Roversi D, Mangoni ML, Stella L. From liposomes to cells: Filling the gap between physicochemical and microbiological studies of the activity and selectivity of host-defense peptides. *Peptide Science.* 2018:e24041.
23. Wimley WC. How does Melittin permeabilize membranes? *Biophys J.* 2018; 114:251–253. [PubMed: 29401422]
24. Wheaten SA, Ablan FD, Spaller BL, Trieu JM, Almeida PF. Translocation of cationic amphipathic peptides across the membranes of pure phospholipid giant vesicles. *J Am Chem Soc.* 2013; 135:16517–16525. [PubMed: 24152283]
25. Zakharov SD, Sharma O, Zhalnina M, Yamashita E, Cramer WA. Pathways of colicin import: utilization of BtuB, OmpF porin and the TolC drug-export protein. *Biochemical Society transactions.* 2012; 40:1463–1468. [PubMed: 23176499]
26. Loh B, Grant C, Hancock RE. Use of the fluorescent probe 1-N-phenyl-naphthylamine to study the interactions of aminoglycoside antibiotics with the outer membrane of *Pseudomonas aeruginosa*. *Antimicrobial Agents and Chemotherapy.* 1984; 26:546–551. [PubMed: 6440475]
27. Lehrer RI, Barton A, Ganz T. Concurrent assessment of inner and outer membrane permeabilization and bacteriolysis in *E. coli* by multiple-wavelength spectrophotometry. *Journal of Immunological Methods.* 1988; 108:153–158. [PubMed: 3127470]
28. Junkes C, Wessolowski A, Farnaud S, Evans RW, Good L, Bienert M, Dathe M. The interaction of arginine- and tryptophan-rich cyclic hexapeptides with *Escherichia coli* membranes. *J Pept Sci.* 2008; 14:535–543. [PubMed: 17985396]
29. Grimm JB, English BP, Chen J, Slaughter JP, Zhang Z, Revyakin A, Patel R, Macklin JJ, Normanno D, Singer RH, Lionnet T, Lavis LD. A general method to improve fluorophores for live-cell and single-molecule microscopy. *Nat Methods.* 2015; 1:2–250. 244–250. 243 p following 250.
30. Los GV, Encell LP, McDougall MG, Hartzell DD, Karassina N, Zimprich C, Wood MG, Learish R, Ohana RF, Urh M, Simpson D, Mendez J, Zimmerman K, Otto P, Vidugiris G, Zhu J, Darzins A, Klaubert DH, Bulleit RF, Wood KV. HaloTag: A novel protein labeling technology for cell imaging and protein analysis. *ACS Chemical Biology.* 2008; 3:373–382. [PubMed: 18533659]
31. Ke N, Landgraf D, Paulsson J, Berkmen M. Visualization of periplasmic and cytoplasmic proteins with a self-labeling protein Tag. *J Bacteriol.* 2016; 198:1035–1043. [PubMed: 26787765]
32. Grimm JB, Muthusamy AK, Liang Y, Brown TA, Lemon WC, Patel R, Lu R, Macklin JJ, Keller PJ, Ji N, Lavis LD. A general method to fine-tune fluorophores for live-cell and in vivo imaging. *Nat Methods.* 2017; 14:987–994. [PubMed: 28869757]

33. Ladokhin AS, White SH. 'Detergent-like' permeabilization of anionic lipid vesicles by Melittin. *Biochimica et Biophysica Acta (BBA) - Biomembranes*. 2001; 1514:253–260. [PubMed: 11557025]
34. Shai Y. Mechanism of the binding, insertion and destabilization of phospholipid bilayer membranes by alpha-helical antimicrobial and cell non-selective membrane-lytic peptides. *Biochim Biophys Acta*. 1999; 1462:55–70. [PubMed: 10590302]
35. Lee MT, Chen FY, Huang HW. Energetics of pore formation induced by membrane active peptides. *Biochemistry*. 2004; 43:3590–3599. [PubMed: 15035629]
36. Yamaguchi S, Hong T, Waring A, Lehrer RI, Hong M. Solid-state NMR investigations of peptide-lipid interaction and orientation of a β -Sheet antimicrobial peptide, Protegrin. *Biochemistry*. 2002; 41:9852–9862. [PubMed: 12146951]
37. Neidhardt FC, Bloch PL, Smith DF. Culture medium for enterobacteria. *J Bacteriol*. 1974; 119:736–747. [PubMed: 4604283]

A. Cecropin A



B. Copolymer MM₆₃:CHx₃₇

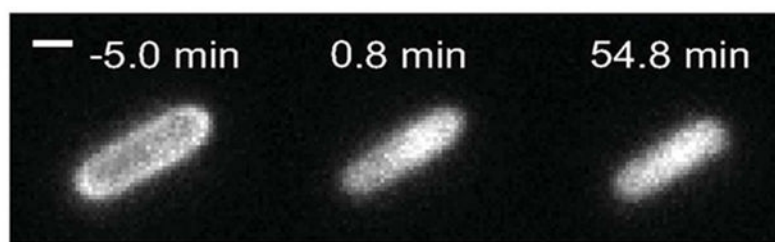
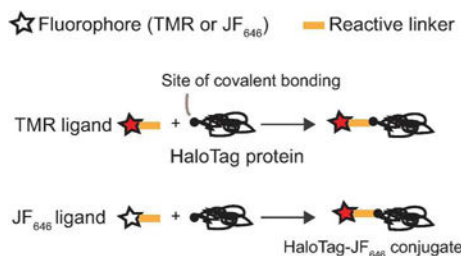


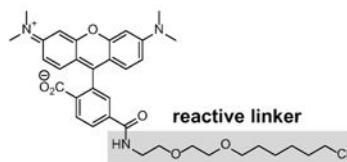
Figure 1. Single-cell, time-lapse assay imaging periplasmic GFP to detect membrane permeabilization events induced in live *E. coli* by antimicrobial agents. **(A)** Cecropin A at 0.9 μM (1X MIC) first induces outer membrane permeabilization to GFP, beginning at the septal region. Initial periplasmic halo image gradually disappears. **(B)** Gellman random β -peptide copolymer MM₆₃:CHx₃₇ at 30 $\mu\text{g}/\text{mL}$ (1.2X MIC) first induces cytoplasmic membrane permeabilization to GFP. Initial periplasmic halo image evolves to a cytoplasmic filled image of which persists for at least 55 min.

A. HaloTag concept

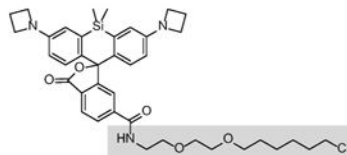


B. Structures of HaloTag agents

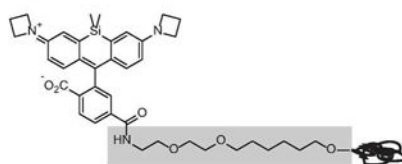
TMR ligand



JF₆₄₆ ligand: mostly lactone



JF₆₄₆-HaloTag conjugate: mostly zwitterion



C. Permeabilization assay

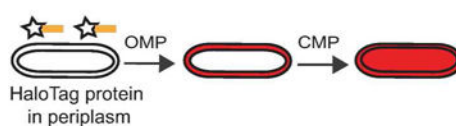


Figure 2. Schematic of HaloTag technique for detection of outer membrane permeabilization (OMP) to small molecules. **(A)** HaloTag ligand consists of a fluorophore (such as TMR) or a profluorophore (such as JF₆₄₆) with a reactive chloroalkane linker (yellow line). HaloTag protein covalently binds to HaloTag ligand through the reactive linker. Free TMR ligand is already fluorescent, whereas JF₆₄₆ ligand fluoresces much more strongly after binding to HaloTag protein. **(B)** Structures of free HaloTag TMR ligand, free HaloTag JF₆₄₆ ligand and HaloTag-JF₆₄₆ conjugate. The structure in the grey area is the reactive linker. **(C)** New OM permeabilization assay uses an *E. coli* strain carrying a plasmid that expresses HaloTag protein with a signal sequence causing efficient export to the periplasm. JF₆₄₆ ligand is not permeable to intact *E. coli*. When an antimicrobial agent induces OMP to small molecules, JF₆₄₆ ligand enters the periplasm, binds to HaloTag protein, and fluoresces in a periplasmic

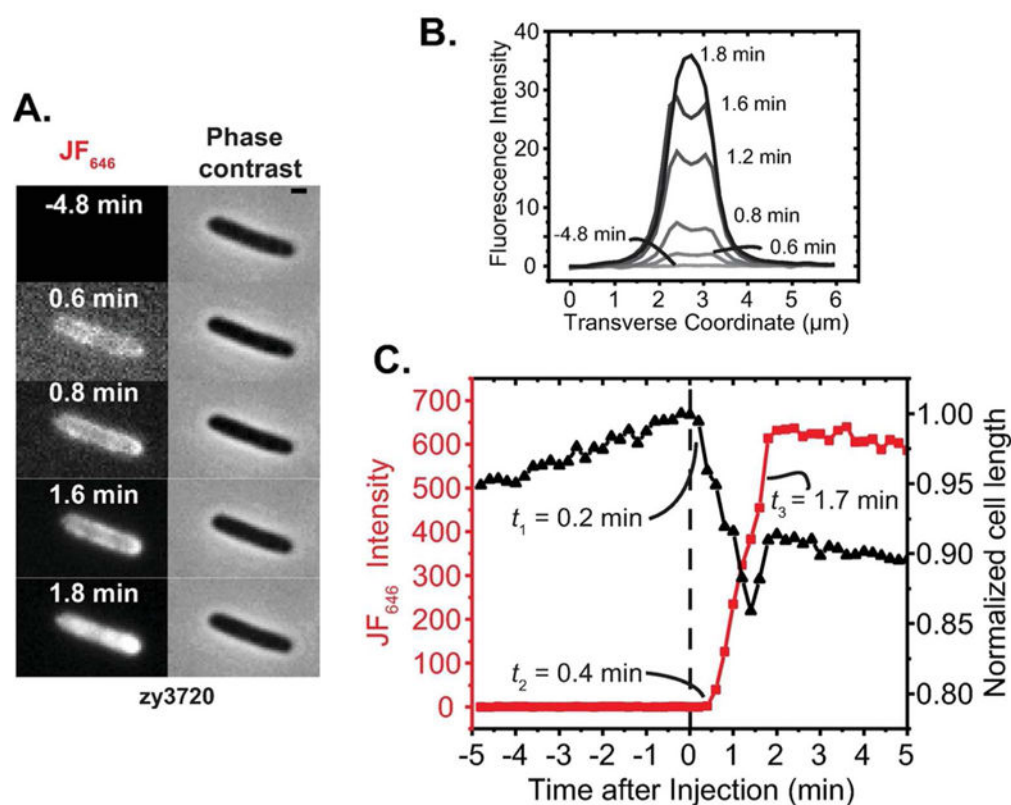
pattern. Subsequent CM permeabilization to globular proteins would cause the pattern to change to that of a filled cytoplasm.

Author Manuscript

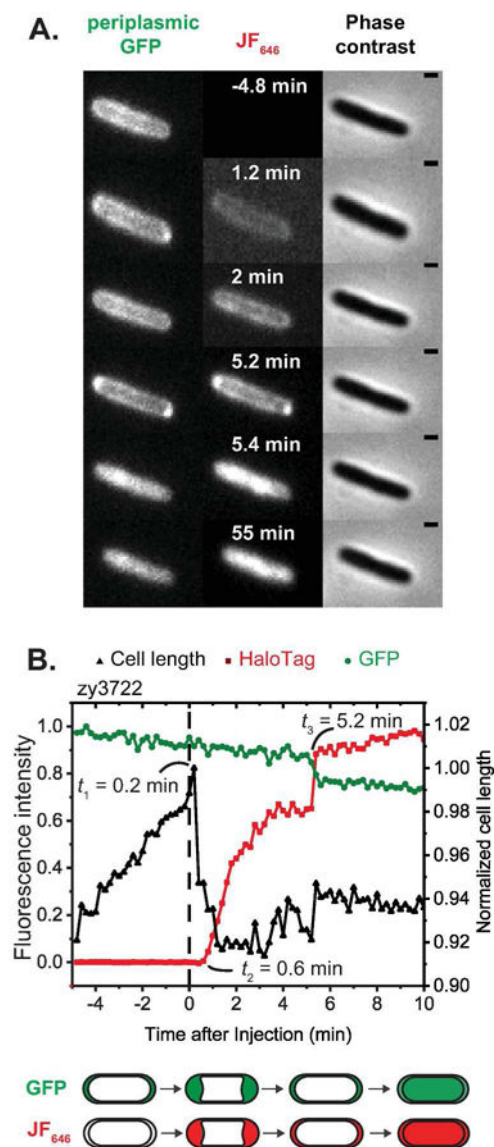
Author Manuscript

Author Manuscript

Author Manuscript

Copolymer $MM_{63}:CHx_{37}$, One-color**Figure 3.**

Application of one-color assay to membrane permeabilization by copolymer $MM_{63}:CHx_{37}$. (A) Red fluorescence and phase contrast snapshots of single *zy3720* E. coli cell following addition of $30 \mu\text{g}/\text{mL}$ $MM_{63}:CHx_{37}$ (1.2X MIC) plus 100 nM JF_{646} ligand at $t = 0$. Time resolution is $12 \text{ sec}/\text{cycle} = 0.2 \text{ min}/\text{cycle}$. Scale bar is $1 \mu\text{m}$. (B) Quantitative transverse intensity profiles vs time. The profile is periplasmic from 0.6 min to 1.6 min and becomes cytoplasmic at 1.8 min. (C) Time dependence of cell length (from phase contrast images) and total HaloTag- JF_{646} fluorescence intensity for the same cell.

Copolymer $MM_{63}:CHx_{37}$, Two-color**Figure 4.**

Application of two-color assay to membrane permeabilization by copolymer $MM_{63}:CHx_{37}$. **(A)** Phase contrast and fluorescence snapshots of single *E. coli* cell expressing periplasmic GFP and periplasmic HaloTag protein, following addition of $30 \mu\text{g/mL}$ $MM_{63}:CHx_{37}$ (1.2X MIC) plus 100 nM JF_{646} ligand at $t = 0$. **(B)** Time dependence of cell length (from phase contrast images) and of GFP and JF_{646} fluorescence intensity for the same cell. Scale bar is $1 \mu\text{m}$.

LL-37, One-color

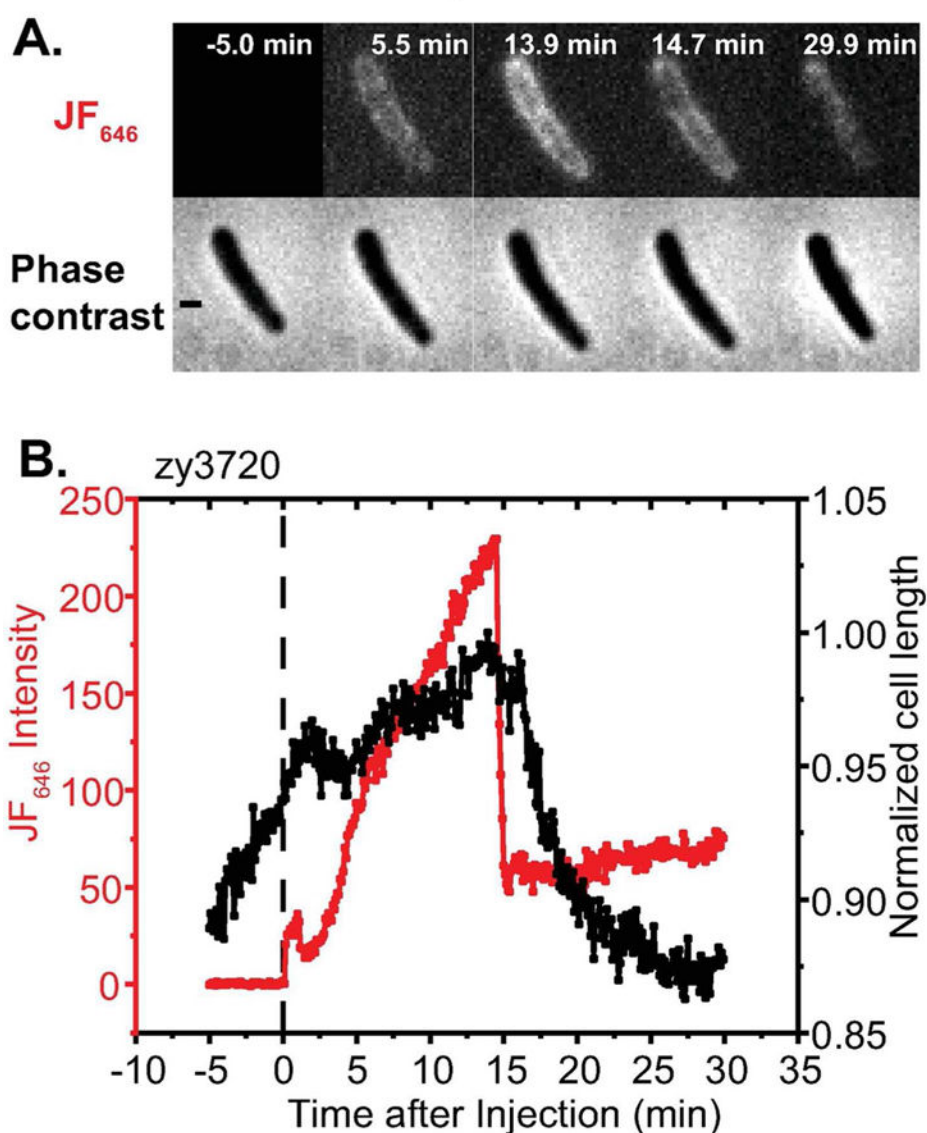


Figure 5. Application of one-color assay to membrane permeabilization by the antimicrobial peptide LL-37. *Top:* Red fluorescence and phase contrast snapshots of single zy3720 *E. coli* cell following addition of 4 μ M LL-37 (1X MIC) plus 100 nM JF₆₄₆ ligand at $t = 0$. Time resolution is 6 sec/cycle = 0.1 min/cycle. *Bottom:* Time dependence of cell length (from phase contrast images) and HaloTag-JF₆₄₆ conjugate fluorescence intensity for the same cell. The fluorescence builds up in the periplasm for ~10 min, prior to the onset of significant cell shrinkage. Abrupt loss of some 75% of the intensity is attributed to OM permeabilization to globular proteins including GFP, HaloTag protein and HaloTag-JF₆₄₆ conjugate. Simultaneous loss of GFP and HaloTag-JF₆₄₆ conjugate was demonstrated in the two-color experiment of Figure S3. Scale bar is 1 μ m.

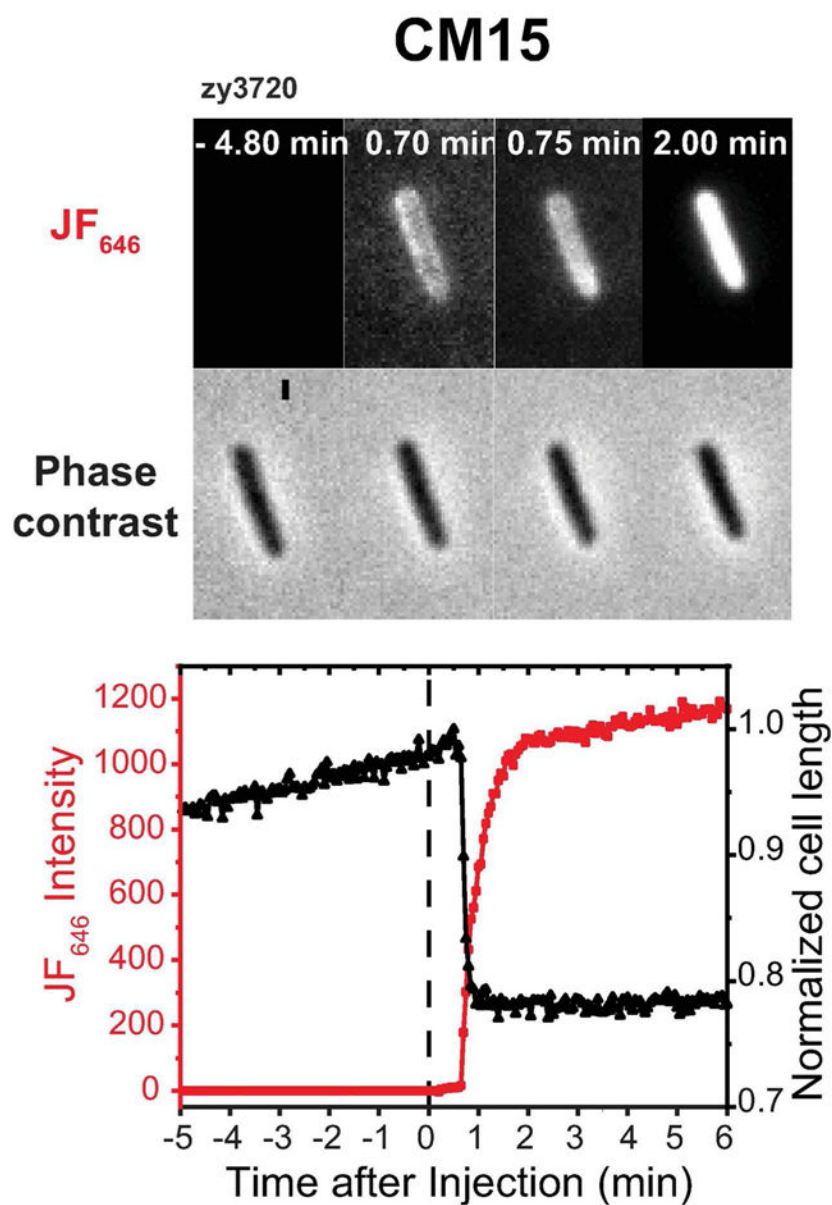
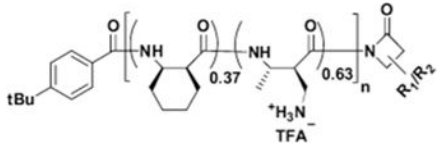


Figure 6.

Application of one-color assay to membrane permeabilization by the antimicrobial peptide CM15. *Top:* Red fluorescence and phase contrast snapshots of single zy3720 *E. coli* cell following addition of 10 μ M CM15 (2X MIC) plus 100 nM JF_{646} ligand at $t=0$. Time resolution is 3 sec/cycle = 0.05 min/cycle. *Bottom:* Time dependence of cell length (from phase contrast images) and HaloTag- JF_{646} fluorescence intensity for the same cell. There is evidence of a transient periplasmic image at 0.70-0.75 min. The onset of red fluorescence and of cell shrinkage are simultaneous within one camera frame (3 sec).

Table 1

Antimicrobial agents.

Antimicrobial Agent	Sequence	Mass (Da)	Net Charge	MIC PM ^I
LL-37	LLGDFFRKSKEKIGKEFKRI-VQRIKDFLRNLVPRTES	4493	+6	4
Cecropin A	KWKLFKKIEKVGQNIRDGII-KAGPAVAVVGQATQIAK-NH ₂	4404	+7	0.9
Melittin	GIGAVLKVLTTGLPALISWI-KRKRQQ-NH ₂	2846	+6	5
β -peptide copolymer ^I MM ₆₃ :CHx ₃₇		~7000	63% cationic sidechains	25 μ g/mL
CM15	KWKLFKKIGAVLKVL-NH ₂	1770	+6	5

^IMinimum inhibitory concentration (in μ M) against WT MG1655 *E. coli* over 6-hr period in aerated EZRDM medium at 30°C, determined by OD for successive two-fold dilutions in 96 well plates. Copolymer MM₆₃:CHx₃₇ lacks a defined molar mass, so MIC is in μ g/mL. The molecular weight of an “average” copolymer is ~7 kDa. Average is 35 subunits long, with 37% CHx (cyclohexyl) and 63% MM (mono-methyl) sidechains; see Ref. 13 for details. Thus an MIC of 25 μ g/mL corresponds to a molar concentration of about 4 μ M.